Applied Catalysis B: Environmental 307 (2022) 121196

Contents lists available at ScienceDirect

Applied Catalysis B: Environmental

journal homepage: www.elsevier.com/locate/apcatb

High-yield electrochemical upgrading of CO_2 into CH_4 using large-area protonic ceramic electrolysis cells

Zehua Pan [a,b,*], Chuancheng Duan [c], Tyler Pritchard [b], Amogh Thatte [b], Erick White [d], Robert Braun [b], Ryan O'Hayre [e,**], Neal P. Sullivan [b,**]

[a] School of Science, Harbin Institute of Technology, Shenzhen, Guangdong 518055, China
[b] Department of Mechanical Engineering, Colorado School of Mines, 1500 Illinois St., Golden, CO 80401, USA
[c] Department of Chemical Engineering, Kansas State University, Manhattan, KA 66506, USA
[d] National Renewable Energy Laboratory, 15523 Denver West Parkway, Golden, CO 80401, USA
[e] Department of Metallurgical and Materials Engineering, Colorado School of Mines, 1500 Illinois St., Golden, CO 80401, USA

ARTICLE INFO

Keywords:
Protonic ceramic electrolysis cells
Electrochemical CO_2 upgrading
Direct high-yield CH_4 production
Electrochemical promotion of catalysis (EPOC)
Energy conversion and storage

ABSTRACT

Electrochemical production of commodity chemicals via CO_2–H_2O co-electrolysis using solid oxide electrolysis cells presents a promising cost-effective energy-storage approach. Here, we harness the unique property of protonic ceramic electrolysis cells (PCEC) and demonstrate direct electrochemical production of CH_4 from CO_2–H_2O in a PCEC unit-cell stack. An exceptional CH_4-yield ratio of 34.6% from only CO_2–H_2O reactants and greater than 70% with exhaust H_2 recycle were achieved under an electrolysis current of –1 A cm^{-2} at 450 °C. Additionally, the electrochemical co-conversion of CO_2–H_2O offered a higher CH_4-yield ratio compared to the thermochemical conversion of CO_2–H_2 under certain operating conditions, indicating possible electrochemical promotion of catalytic CO_2 methanation. Techno-economic analyses were conducted to reveal potential operating conditions that yield a promising levelized cost of fuel production. The demonstrated good performance of the unit-cell stack shows promising scalability of PCECs for practical application from a system-level viewpoint.

1. Introduction

The market emergence of site-specific and intermittent renewable energy sources, such as wind and solar energy, necessitates the development of energy-storage technologies. Energy storage in the form of economically fungible chemical fuels potentially provides a low-cost grid-balancing solution for renewables penetration. Solid oxide electrolysis cells (SOECs) can efficiently electrochemically upgrade water and/or carbon dioxide and produce commodity chemicals, such as hydrogen, syngas or hydrocarbon fuels, for future on-demand power generation [1,2]. The chemical fuels can be either compressed and stored in tanks, or directly transported through pipelines, enabling large storage capacity and nearly infinite energy-storage duration. Here we harness the unique properties of protonic ceramic electrolysis cells (PCECs) for electrochemical CO_2 upgrading to a commodity chemical, CH_4, that can be easily transported to end-users for subsequent on-demand power generation. This energy-storage solution brings the added benefit of CO_2 reuse and the potential alleviation of greenhouse gas emissions.

Although energy storage with H_2 as the energy carrier has been widely studied, the use of CH_4 as the energy carrier brings thermodynamic and performance advantages [3–5]. Major hurdles facing hydrogen include its low volumetric energy density, the need for safe and cost-effective storage and transportation solutions, and its limited compatibility with existing infrastructure, such as natural gas pipelines and end-use appliances [6]. Methane handling is more straightforward; the CH_4-based product gas can be directly introduced into the existing natural gas infrastructure. Most importantly, using CH_4 as an energy carrier enables a higher cell-level thermodynamic maximum round-trip efficiency ($\varepsilon_{RT,max}$) in comparison to H_2 [7,8]. As shown in Fig. 1a, theoretical $\varepsilon_{RT,max}$ for the H_2-based energy storage decreases nearly linearly with increasing temperature, reaching 76% at 800 °C near the operating temperature of SOECs. In contrast, theoretical $\varepsilon_{RT,max}$ is nearly 100% and temperature-invariant for CH_4-based energy storage. The wide, high-efficiency operating window also brings a measure of system robustness.

* Corresponding author at: School of Science, Harbin Institute of Technology, Shenzhen, Guangdong 518055, China.
** Corresponding authors.
E-mail addresses: panzehua@hit.edu.cn (Z. Pan), rohayre@mines.edu (R. O'Hayre), nsulliva@mines.edu (N.P. Sullivan).

https://doi.org/10.1016/j.apcatb.2022.121196
Received 31 October 2021; Received in revised form 14 January 2022; Accepted 5 February 2022
Available online 8 February 2022

Methane production through co-electrolysis of CO_2 and H_2O has been demonstrated with oxygen-ion-conducting SOECs (O-SOECs) [9–13]. During operation, CO_2 and H_2O feedstocks are co-fed to the fuel electrode, where water vapor is electrolyzed and oxygen ions are driven across the electrolyte. This leaves H_2 at the fuel electrode to facilitate CO_2 reduction through the reverse water-gas shift reaction:

$$CO_2 + H_2 = CO + H_2O\ (\Delta H_{298} = 41\ \text{kJ mol}^{-1})\cdot \quad (1)$$

Methane is formed through CO/CO_2 hydrogenation:

$$CO + 3H_2 = CH_4 + H_2O\ (\Delta H_{298} = -206\ \text{kJ mol}^{-1}), \quad (2)$$

$$CO_2 + 4H_2 = CH_4 + 2H_2O\ (\Delta H_{298} = -165\ \text{kJ mol}^{-1}), \quad (3)$$

with Rx. (3) known as the Sabatier reaction. The integration of exothermic methane production with the endothermic water electrolysis in a single device enables in-situ heat balancing to boost conversion efficiency. Further, the integration simplifies the system, facilitates thermal management, and improves reliability.

Li, et al. [9] attempted to achieve direct CH_4 production utilizing an O-SOEC with conventional nickel/yttria-stabilized zirconia (Ni-YSZ) fuel electrode material set. With a feedstock of 50 mL min^{-1} H_2O and 25 mL min^{-1} CO_2 to fuel electrode, a CH_4-yield ratio of 0.03% (where the CH_4 yield ratio is defined as the CH_4 production / CO_2 feed) was obtained under a total electrolysis current of –0.608 A at 550 ℃. Luo, et al. [11] reported a similar CH_4-yield ratio of 0.03% by using a tubular O-SOEC with the same Ni–YSZ fuel electrode at 600 ℃ under a total electrolysis current of –0.97 A. Featuring a novel Fe–$La_{0.2}Sr_{0.8}TiO_{3-\delta}$ fuel electrode, Xie, et al. [10] demonstrated an improved CH_4-yield ratio of 0.2% at 650 ℃ with a feedstock of 2 mL min^{-1} H_2O and 1 mL min^{-1} CO_2.

These low CH_4-yield ratios are rooted in the typical high (700–900 °C) operating temperatures of O-SOECs, at which the exothermic methanation reactions are not thermodynamically favored (Fig. S1a). Additionally, co-feeding H_2O with CO_2 drives the methanation reaction towards the reactants through Le Chatelier's principle

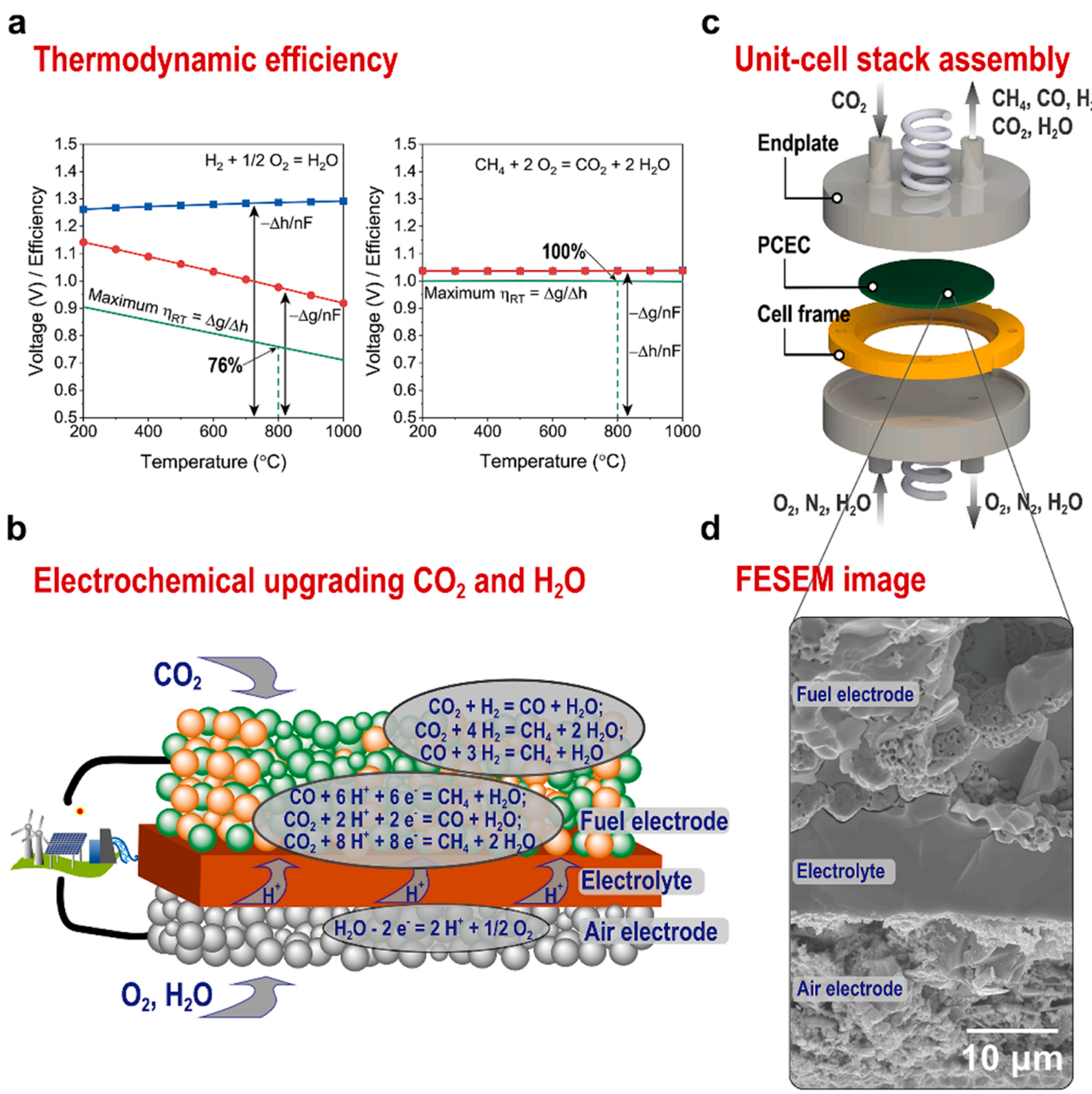

Fig. 1. Illustration of PCEC unit-cell stack for CO_2–H_2O co-conversion. a, Comparison of theoretical thermodynamic cell-level maximum round-trip efficiency, $\varepsilon_{RT,max}$, between H_2-based (left) and CH_4-based (right) energy storage options. b, Schematic illustration of the possible electrochemical and chemical reactions in the PCEC during upgrading CO_2–H_2O into CH_4. CO_2 reduction may occur via the direct electrochemical pathway where adsorbed protons and electrons reduce CO_2 directly, or by the indirect pathway where CO_2 is thermochemically hydrogenated by electrochemically generated H_2. c, Unit-cell stack assembly of the PCEC. The cell is bonded into a ceramic frame and then sandwiched by two ferritic-steel endplates. (See Fig. 2 for detailed pictures of the assembly) d, Cross-sectional morphology of a freshly prepared and reduced PCEC.

(Fig. S1c). To facilitate CH_4 production, supplying additional H_2 has proved to be effective [9,11], in agreement with thermodynamic predictions (Fig. S1b). For instance, Luo, et al. [11] improved the CH_4-yield ratio from 0.03% to 12% by switching the reactant to a 1:1:1 gas mixture of CO_2–H_2O–H_2 while keeping other operating conditions the same. Further, Chen, et al. [12] and Lei, et al. [13] exploited the tubular cell architecture to create two distinct high- and low-temperature zones along the O-SOEC, with the former for high-efficiency H_2O electrolysis, and the latter for high-selectivity methanation. Combined with supplemental H_2, these innovations increased the CH_4-yield ratio to 41% [12] and 84% [13], respectively. However, the split-zone approach engenders thermo-mechanical stresses to the delicate electro-ceramic cell components and brings reliability concerns. Co-feeding extra H_2, the amount of which cannot be fulfilled by recycling exhaust H_2 [11–13], also requires substantial cost and energy input for hydrogen production.

Alternatively, PCECs recently emerge as a novel type of SOEC for the production of chemical fuels [14–19]. During water electrolysis, Duan, et al. [14], Choi, et al. [15] and Vollestad, et al. [16] have separately attested hundreds to thousands of hours of stable operation with high Faradaic efficiencies, with scale-up to multi-cell stacks now underway [17]. PCECs also offer several important benefits integral to achieving high-efficiency direct CH_4 production. The small size of the protonic charge carrier enables higher ionic conductivity at lower operating temperatures (400–600 °C) in comparison to O-SOECs. These lower temperatures present a better balance between the thermodynamics of the Sabatier chemistry favored at a lower temperature, and the chemical kinetics of CO_2 conversion and CH_4 formation favored at a higher temperature [20]. Most significantly, protonic ceramics provide physical separation of the CO_2 and H_2O feedstocks at opposing electrodes, as illustrated in Fig. 1b. Higher CO_2 conversions have been demonstrated in sorption-enhanced [21] and membrane reactors [22], where timely removal/adsorption of product water shifts the thermodynamic equilibrium of methanation reaction towards the products. The physical separation in the PCEC presents a similar condition; protons formed through H_2O electrolysis at the air electrode serve as the H_2 source for CO_2 hydrogenation at the fuel electrode, eliminating the existence of reactant H_2O in the fuel electrode and facilitating higher CH_4 production.

Researchers are now harnessing protonic ceramics to directly produce CH_4 from CO_2 and H_2O, with significant improvement on the CH_4-yield ratio observed. Xie, et al. [23] employed a protonic ceramic membrane as a hydrogen pump to produce CH_4 from CO_2 and H_2 with a yield ratio of 1.4% using a fuel electrode composed of Fe and $BaCe_{0.5}Zr_{0.3}Y_{0.16}Zn_{0.04}O_{3-\delta}$ at 614 °C. Li, et al. [24] also demonstrated a thermo-electrochemical production of C_1 species with a similar approach from H_2 and CO_2. By tuning of the Ir–O hybridization of the Ir–ceria-based catalysts, a CH_4 selectivity of nearly 100% was achieved. Duan, et al. [14] demonstrated the direct synthesis of CH_4 from only CO_2 and H_2O reactants using a small (0.5 cm^2 active area) PCEC "button cell", reaching a CH_4-yield ratio of 7.5% at 500 °C with a total electrolysis current of –1.625 A. While this is much higher than the previous 0.2% CH_4-yield ratio obtained from O-SOECs, still higher yield ratios are needed for commercialization.

The fundamental electrochemical and thermochemical processes underway during protonic-ceramic electrolysis of CO_2 are also unclear. As shown in Fig. 1b, the potential role of direct electrochemical CO_2 reduction from protons, and its interplay with thermochemical CO_2 reduction from electrochemically produced H_2, warrant further study. The difference is important as the electric field could possibly promote the reaction, which is referred to as the electrochemical promotion of the catalysis (EPOC) effect [25–28]. Jiménez, et al. [26] found that with Ni or Ru catalyst supported on YSZ, the CH_4 formation rate during CO_2 hydrogenation increased from 0.90×10^{-8} mol s^{-1} to 0.99×10^{-8} mol s^{-1} upon the application of a negative potential of -1.30 V. Recently, Zagoraios, et al. [27] and Kalaitzidou, et al. [28] have also observed promotion of the CO_2 hydrogenation process with Ru nanoparticles supported on proton-conducting yttria-doped barium zirconate electrolyte under bias. However, to the authors' knowledge, direct comparison between electrochemical and thermochemical CO_2 upgrade in PCECs during CO_2–H_2O co-conversion has not been quantitatively investigated.

Motivated by the potential operational benefits brought by protonic ceramics, here we successfully fabricated and assembled larger-area (5 cm^2 active area) PCEC unit-cell stacks (Fig. 1c). Comparing with previous lab-scale button cell study, the unit-cell stack as developed, composed of one cell and two endplates, enables more-efficient utilization of reactants and the evaluation of the performance from a broader system-level viewpoint in practical application. The fuel-cell-mode operation with humidified CH_4 was first conducted to attest the scalability of the protonic ceramic cells. Afterwards, direct CH_4 production through electrochemical CO_2–H_2O co-conversion was characterized and promising CH_4-yield ratios were demonstrated. Additionally, a direct comparison was made between the electrochemical conversion of CO_2–H_2O and the thermochemical conversion of CO_2-H_2 using the same cell. We find that in some conditions, this electrochemical CH_4-synthesis route gives a higher CH_4 yield than the thermochemical route, demonstrating a possible EPOC effect. Lastly, techno-economic analyses were conducted to identify system-scale operating conditions that present an encouraging levelized cost of fuel production.

2. Experimental

2.1. Fabrication of 5–cm^2 PCECs

The fuel electrode-supported planar PCECs were prepared following the solid-state reactive sintering (SSRS) process [29]. Detailed powder synthesis and cell fabrication processes can be found in the Supplemental Material and the cross-sectional image of a freshly prepared and reduced cell is shown in Fig. 1d. The morphology was examined using Field Emission Scanning Electron Microscopy (FESEM, JSM-7000F). The cell has a $BaCe_{0.4}Zr_{0.4}Y_{0.1}Yb_{0.1}O_{3-\delta}$ (BCZYYb) electrolyte with a thickness of ~ 8 μm. The ~0.8-mm-thick fuel electrode is composed of 60 wt% NiO and 40 wt% BCZYYb together with an additional 20 wt% starch. The air electrode is made of 80 wt% $BaCo_{0.4}Fe_{0.4}Zr_{0.1}Y_{0.1}O_{3-\delta}$ (BCFZY) and 20 wt% BCZYYb.

2.2. Assembly of a 5–cm^2 PCEC unit-cell stack

The schematic diagram of the unit-cell stack is presented in Fig. 1c and the photographs can be found in Fig. 2. The PCEC cell (Fig. 2a) was bonded into a ceramic frame with fuel electrode facing up and sealed using a ceramic bond paste (Ceramabond 552, Aremco Products Inc.) as shown in Fig. 2b top. The frame was then sandwiched by two identical metal endplates (Fig. 2c), made of Crofer 22 APU, and the sealing was achieved by vermiculite under compression force applied from a hydraulic jack (not shown) installed on the test stand (Fig. 2d). The gap between the fuel electrode and the endplate is ~ 2.5 mm in the assembly. The current collection was achieved via silver wires and paste (Fig. 2b top). The dimensions of the ceramic frame and the endplate are shown in Fig. S2.

2.3. Performance characterization of PCEC unit-cell stack

Electrochemical characterization was performed on a custom electrochemical test stand. The desired gas composition was achieved by regulating the supply of gases from individual gas cylinders using mass flow controllers. A heated bubbler was used to provide the desired steam flow by adjusting the set temperature. Current−voltage ($I-V$) and electrochemical impedance spectroscopy (EIS) measurements were performed using a Gamry Interface 5000E. EIS was carried out over a frequency ranging from 100 kHz to 0.1 Hz with an AC amplitude of 10 mV under open-circuit voltage (OCV).

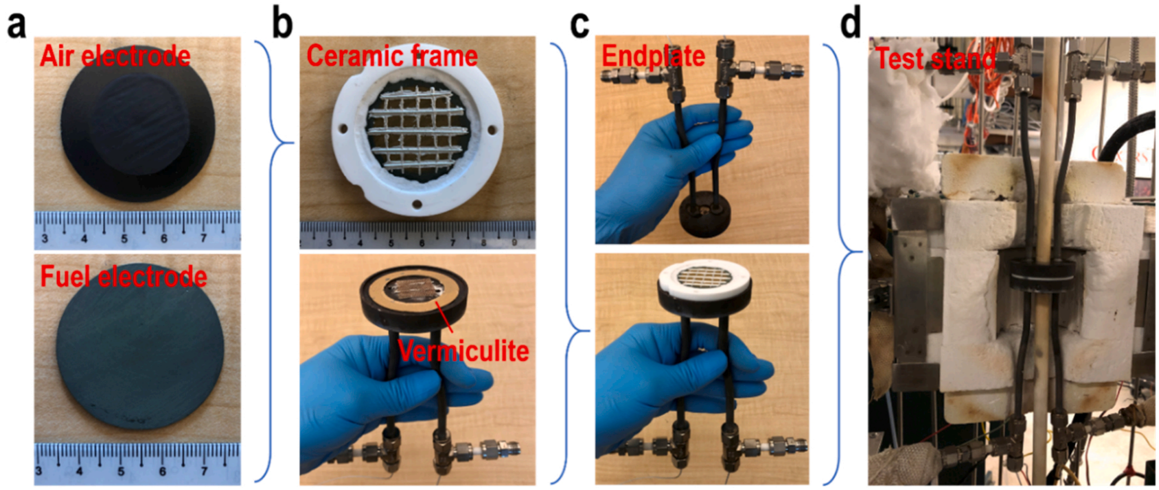

Fig. 2. Pictures of the PCEC unit-cell stack and the test station. a, the as-prepared PCEC cell; b and c, the unit-cell stack assembly; d, the test stand (The compression force was applied from a hydraulic jack (not shown) on the cell with the two alumina tubes).

In direct-CH_4-fueled fuel-cell mode, the $I-V$ curves were obtained across a range of temperatures with a mixture of 20 sccm CH_4, 80 sccm N_2 and 67 sccm steam as the fuel to produce a steam-to-carbon ratio = 3.35. The high N_2 flow rate is to reduce the steam concentration and minimize fluctuations in steam flow rate, but likely to decrease the cell performance due to the fuel-dilution effect.

During electrochemical CO_2-H_2O co-conversion, the air electrode was supplied with 200 sccm synthetic air with 20% steam and the fuel electrode was fed with 48 sccm N_2 and 2 sccm CO_2. The 4% CO_2 concentration in the stream was selected to be consistent with previous tests on button cells [14]. This feedstock results in H_2-to-CO_2 ratios ranging from ~ 2:1 to ~ 6:1 in the fuel electrode stream depending on the electrolysis current density. Current densities varied from − 0.4 A cm^{-2} to − 1 A cm^{-2} with an interval of 0.1 A cm^{-2} were applied and kept for 1 h for each step. The fuel-electrode exhaust gas flow was monitored by a gas flow calibrator (Defender 530 +, Mesa Labs) and a gas chromatograph (3000 Micro GC, Agilent). Any steam content in the exhaust gas flow was removed by calcium sulfate desiccant (W. A. Hammond DRIERITE Co. LTD) prior to the gas flow calibration and gas chromatography. Calculation of Faradaic efficiencies (FEs) is detailed in the Supplemental Material. The Faradaic efficiency towards all the products is denoted as FE_{total}, while FE_{CH4} indicates the Faradaic efficiency towards CH_4 production.

The thermochemical CH_4 synthesis was conducted by co-feeding H_2 and CO_2 into the fuel-electrode chamber while keeping all other operating parameters the same as those used in electrochemical CH_4 synthesis. The flow rate of CO_2 and N_2 were kept at 2 sccm and 48 sccm, respectively, while the flow rate of H_2 was varied.

2.4. Techno-economic analysis

To identify system-scale operating conditions, the economic performance of the electrochemical CO_2 upgrade with PCECs was evaluated using a levelized cost of fuel production (LCOFP) analysis. Detailed analysis procedures can be found in the Supplemental Material.

3. Results and discussion

3.1. PCEC performance in fuel-cell mode with humidified CH_4

The electrochemical performance of the unit-cell stack was first characterized in fuel-cell mode with humidified CH_4 fuel (Fig. 3). The open-circuit voltage (OCV) ranged from 1.02 (at 550 °C) to 1.04 V (at 400 °C), indicating good quality of the large-area cell and adequate gas

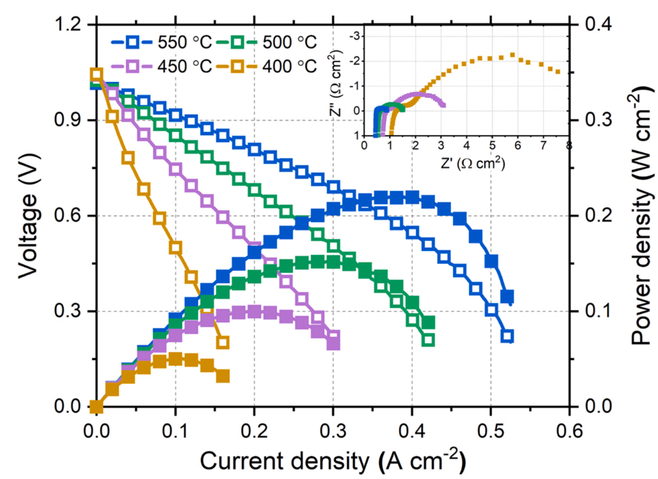

Fig. 3. Current-voltage and current-power characterization of the protonic ceramic unit-cell stack in CH_4-fueled fuel-cell mode with electrochemical impedance spectra shown in the inset.

sealing within the stack package. Peak power densities were demonstrated to be 0.22, 0.15, 0.10 and 0.05 W cm^{-2} at 550, 500, 450 and 400 °C, respectively. Higher performance can be obtained through a higher-temperature operation that facilitates CH_4 reforming and electrochemical reaction [30]. Also, as mentioned earlier, the high N_2 concentration used here likely decreased the performance due to fuel-dilution effects. The area-specific ohmic and polarization resistances at 550 °C reached 0.48 and 0.41 Ω cm^2. These results are comparable with previously demonstrated state-of-the-art performances for small protonic ceramic button cells (0.5 cm^2 active area) [29,31], though the electrochemically active area has been increased in this case by an order of magnitude. The larger cell size and packaging within a conventional SOFC-stack material set demonstrates an encouraging measure of device scalability.

3.2. PCEC performance in electrolysis mode for CO_2–H_2O co-conversion

Electrochemical polarization curves and methane-production rates during CO_2 −H_2O co-conversion are shown in Fig. 4. In order to achieve an electrolysis current density of –1 A cm^{-2}, the applied voltages were 1.36, 1.50, 1.63 and 1.78 V at 550, 500, 450 and 400 °C, respectively. Peak CH_4 production was achieved at 450 °C under –1 A cm^{-2} with a

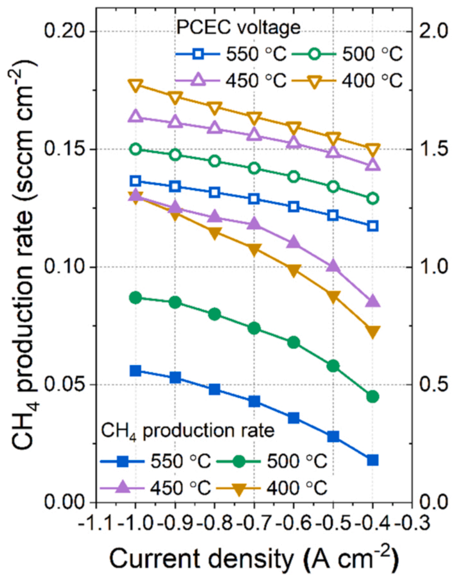

Fig. 4. Characteristic current−voltage curves and methane production rates for CO_2–H_2O co-conversion with the PCEC unit-cell stack as a function of current density at different temperatures. The flow rate of CO_2 to the fuel-electrode chamber is 2 sccm, carried by 48 sccm N_2.

production rate of 0.13 sccm cm^{-2}. The non-linear increase of the methane production rate with increasing current density is in agreement with the thermodynamic predictions for the CH_4 yield with an increasing H_2-to-CO_2 ratio (Fig. S1b). Methane production is also highly temperature sensitive; CH_4 production at 400–450 °C is more than double the value found at 550 °C. Further, the CH_4 formation is steady between 400 and 450 °C, presenting a wide and robust operating window. This result experimentally validates the potential application of protonic-ceramic electrolyzers for CO_2 upgrading into practical fuels.

3.3. *Performance metrics of in-situ CH_4 production during CO_2–H_2O co-conversion*

Fig. 5 shows the evolution of the cell voltage and product-gas composition with a stepwise increase in the applied current density during CO_2−H_2O co-conversion. Both the cell voltage and the CH_4, CO and H_2 product yields are reasonably stable at each current density. The ratios of carbon out to carbon in were calculated and the result is shown in Fig. S3. Mostly, the ratio falls in the range of 92–95%, which could be due to the fact that other possible products such as C_{2+} fuels were not monitored. Further, no morphological damages can be observed from post-mortem analysis of PCEC electron micrographs (Fig. S4). These observations establish at least the short-term stability of the cell.

The CH_4 production performance metrics, CO_2 conversion, CH_4 selectivity and CH_4-yield ratio, are shown in Fig. 6. Because of the exothermic nature of CO_2 methanation, lower operating temperatures are thermodynamically favorable but kinetically unfavorable. As shown in Fig. 6a and b, this interplay leads to increasing CO_2 conversion but decreasing CH_4 selectivity with increasing temperature. Reflecting the tradeoff between these two factors, the CH_4-yield ratio increased first from 14.5% to 34.6% when the operating temperature decreased from 550 °C to 450 °C, and then decreased to 32.7% at 400 °C (Fig. 6c), with an electrolysis current of –1 A cm^{-2}. Overall, the CH_4-yield ratio is maximized to 34.6% at an intermediate temperature of 450 °C; to the authors' knowledge, this is the highest electrochemical CH_4-yield ratio from CO_2–H_2O co-conversion reported to date. Apart from the lower operating temperature of the PCEC, the high CH_4-yield ratios are also a result of the physical separation of the CO_2 and H_2O feedstocks at opposing electrodes. Fig. S5 compares the performance metrics of CO_2–H_2O co-conversion with and without additional 5% steam in the gas stream supplied to the fuel electrode. The CH_4-yield ratio decreases from 16.8% to 6.6% under a current density of –1 A cm^{-2} at 550 ℃ upon the addition of steam. This result agrees with our thermodynamic predictions (Fig. S1c) and previous reports [21,22]. Lastly, the CH_4-yield ratio increased with the increasing current density, as a result of increasing H_2-to-CO_2 ratio. We hypothesize that higher current densities could further facilitate CH_4 production.

Fig. 6d demonstrates the change of CO_2 conversion, CH_4 selectivity and CH_4-yield ratio with the increase of the equivalent H_2-to-CO_2 ratio at 450 °C. Equivalent H_2-to-CO_2 ratios were calculated by dividing the equivalent H_2 flow rate in the exhaust stream, $\dot{V}_{H_2,eq}$ (Eq. S2), by the flow rate of input CO_2. When the equivalent H_2-to-CO_2 ratio increased from 3.14 to 5.35 by imposing higher current densities, the CH_4-yield ratio increased from 23.2% to 34.6%. Previously, the CH_4-yield ratio during CO_2–H_2O co-conversion was reported to be 7.5% with an equivalent H_2-to-CO_2 ratio of around 5: 1 [14]. In comparison, the CH_4-yield ratio reached 33.7% in this work under the same H_2-to-CO_2 ratio, demonstrating the promising applicability of PCEC in electrochemical CO_2 upgrade with a practical stack assembly.

The FEs of the cell during CO_2–H_2O co-conversion are shown in Fig. S6. Protonic-ceramic materials are mixed ionic-electronic conductors. The incorporation of molecular oxygen into oxygen vacancies in oxidizing environments will result in the formation of electron holes [32–34]. This leads to non-negligible electronic conductivity and reduces the transference number of protons. Therefore, the actual protonic current density in the electrolyte is smaller than the applied external electrolysis current density. In short, the formation of electron holes negatively affects the FE. In proton-conducting BCZYYb ceramic, the concentration of electron holes can be related to operating conditions, such as oxygen and steam partial pressures, through the water oxidation equilibrium via [16,35]:

$$[h^{\bullet}] = K\left[OH_O^{\bullet}\right]\left[O_O^{\times}\right]p_{H_2O}^{-\frac{1}{2}}p_{O_2}^{\frac{1}{4}}, \quad (4)$$

assuming full hydration. The FE_{total} was calculated to be in the range of 20%– 50% (Fig. S6a); this is reflective of the relatively oxidizing nature of these two feedstocks. During water electrolysis, researchers have demonstrated high FEs [14–16]. Further efforts will be spent on improving the FEs during CO_2–H_2O co-conversion. The FE_{CH4} is shown in Fig. S6b. A maximum value of 12% was obtained at 450 °C, consistent with the optimal operating temperature for CH_4 synthesis.

Generally, the FE_{total} decreased with increasing electrolysis current density. This could be a result of the consumption of steam and the production of oxygen at higher electrolysis current densities, which lowers the local p_{H_2O} and increases the local p_{O_2} at the air electrode. Further, the FE_{total} decreased with decreasing operating temperature. This is in contrast to the theoretical predictions based on the transportation properties of protonic ceramics [33,34,36]. However, the polarizations occurring at the electrodes and the choices of both the electrolyte and electrodes may greatly affect the cell performance [14–16]. More efforts are needed to comprehensively investigate the transportation behaviors of protonic ceramics during CO_2–H_2O co-conversion.

Further attempts were made to boost the CH_4-yield ratio. As a first step in this direction, we achieved an improvement on CH_4-yield ratio from 34.6% to 40.9% at 450 ℃ (Fig. S7a) by increasing the electrolyte thickness from ~8 to ~12 μm. Through modeling approach, Nakamura, et al. [37] and Qiu, et al. [38] have demonstrated that increasing the electrolyte thickness can suppress leakage current and is beneficial for the improvement of the FE in the fuel-cell mode. Zhang, et al. [39] also experimentally demonstrated that a thicker electrolyte would lead to a higher open-circuit voltage. Considering the strong oxidizing environment at the air electrode, the electron-hole formation mainly takes place at the air electrode side of the electrolyte. Due to the thin electrolyte used, it is speculated that the hole formation dominates the

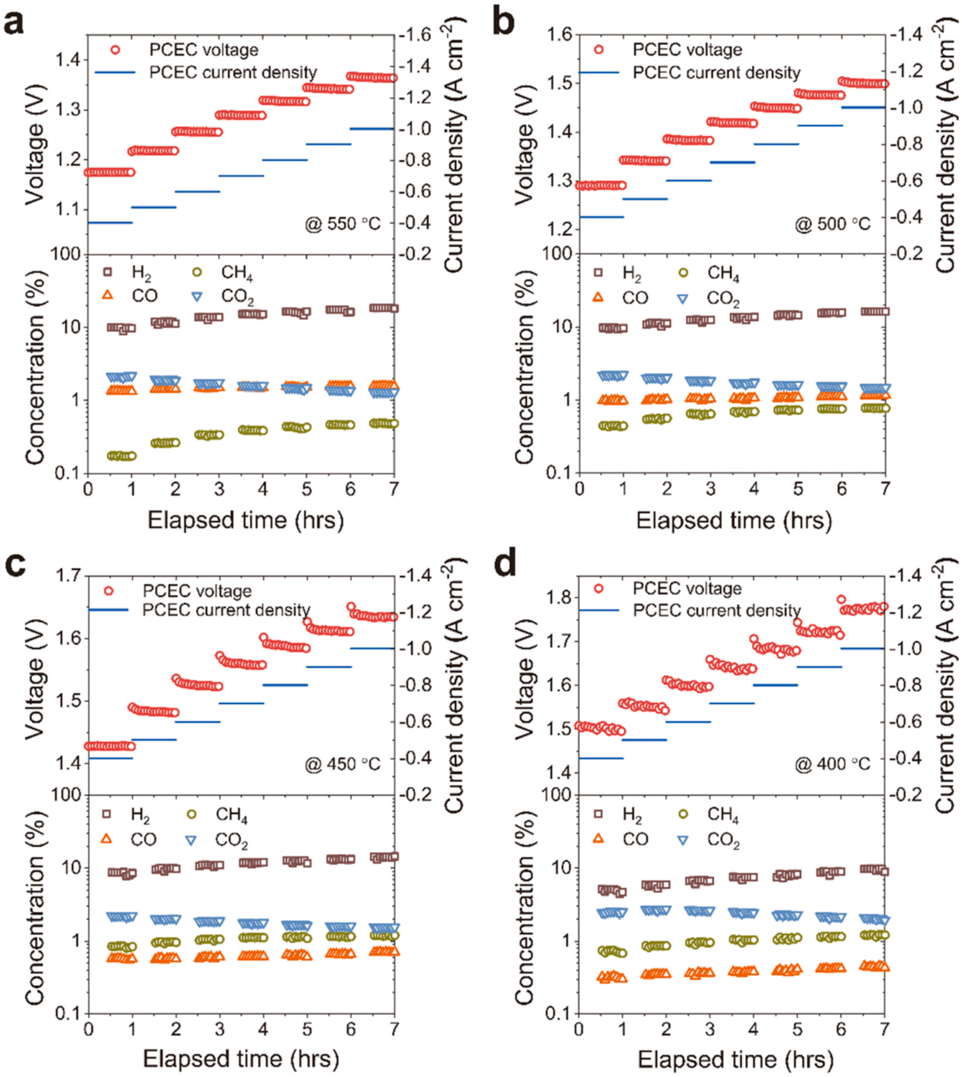

Fig. 5. Evolution of voltage and exhaust gas concentrations with elapsed time of the PCEC during CO_2−H_2O co-conversion at different temperatures. Stable voltage and exit gas composition at each current density demonstrate the short-term stability of the cell. Electron micrographs of the cell before and after the operation shown in Fig. S4 reveal no morphological damage.

electron-hole concentration profile. Thus, increasing the thickness of the electrolyte while keeping other parameters the same will lower the electron-hole concentration at the fuel-electrode side and improve the FE. Fig. S8 shows the EIS of the two cells tested at 550 ℃. The ohmic resistance increased from 0.31 Ω cm^2 to 0.44 Ω cm^2 as a result of the thicker electrolyte. Consequently, Fig. S7c shows that the FE_{total} was improved from 30.6% to 39.8% at a current density of − 1 A cm^{-2}, leading to higher H_2 production rates and thus a higher CH_4-yield ratio. Meanwhile, the cell voltage was increased by ~4%, from 1.63 V to 1.72 V (Fig. S7b), indicative of the increased DC resistance brought with the thicker electrolyte. Nonetheless, the effect of electrolyte thickness on the FE warrants further detailed investigation.

Alternatively, increasing the H_2-to-CO_2 ratios by recycling exhaust H_2 to the fuel electrode together with the CO_2 feed enables a significant increase in the CH_4-yield ratio, from 34.6% to 71.2% at 450 ℃ with an electrolysis current of –1 A cm^{-2} (Fig. 7a), marking a 106% improvement. In the experiment, supplemental H_2 with a flow rate lower than the flow rate of H_2 in the exhaust gas stream (Fig. 7c) was provided. Thus, assuming that efficient downstream separation of CH_4 and H_2 can be executed, the supplemental H_2 demand can be met by recycling electrochemically produced H_2, without the need for external H_2 supply. The supply of recycled H_2 also suppresses hole formation [33], and therefore improves the FE_{total} of the stack under the same current density (Fig. 7b). A comparison between the performance with and without recycling exhaust H_2 against equivalent H_2-to-CO_2 ratio is shown in Fig. 7d. It can be seen that the CH_4-yield ratios show higher values with H_2 recycle, benefitting from the parallel routes of thermochemical and electrochemical CO_2 methanation. These effects synergistically improve the stack energy density and energy efficiency. As will be shown, the performance improvements brought by H_2 recycle also substantially decrease the LCOFP.

Overall, in a practical stack configuration, the PCEC enables a CH_4-yield ratio of 34.6% without H_2 recycle and 71.2% with H_2 recycle. As found in Table S1–S2, these values exceed the previously reported values of 0.3–7.5% from direct CO_2 and H_2O co-conversion using button cells [9,10,14,23], and are comparable to previous values ranging from 12% to 84% with external H_2 supply using button cells or with two distinct temperature zones using tubular cells [3,9,11–13]. The much–improved CH_4-yields presented here compared with the previous lab-scale button-cell tests demonstrate a promising result for future upscale and practical application of PCECs.

Compared with CO_2 reduction and CH_4 production in the aqueous system, the work here shows a higher areal CH_4 production rate, while maintaining a similar FE_{CH4} (Table S3). The highest CH_4 production rate

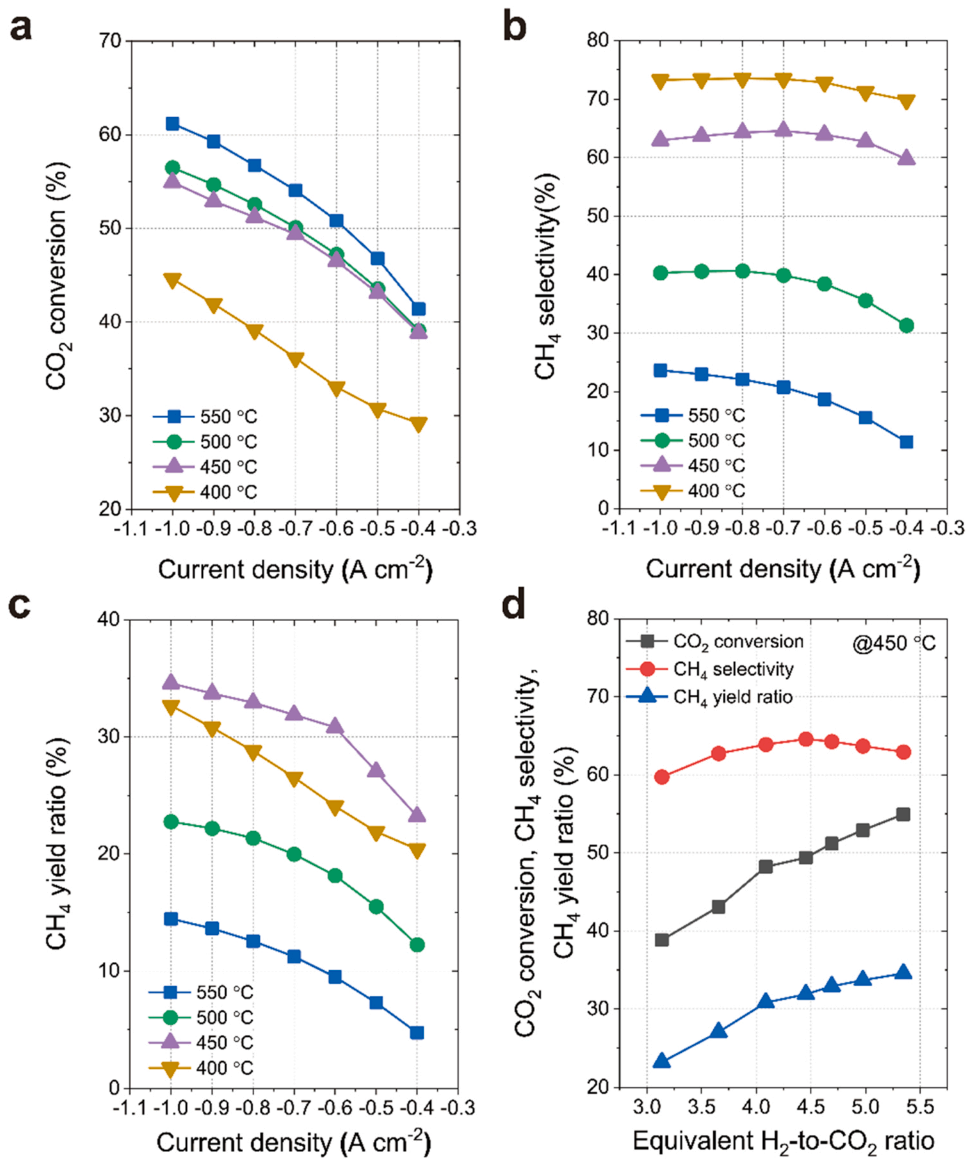

Fig. 6. CO_2 conversion metrics of the PCEC during CO_2–H_2O co-conversion. a–c, Dependence of CO_2 conversion, CH_4 selectivity and CH_4 yield ratio on the current density at different temperatures. d, Dependence of CO_2 conversion, CH_4 selectivity and CH_4 yield on the equivalent H_2 ($\dot{V}_{H_2,eq} = \dot{V}_{H_2} + \dot{V}_{CO} + 4 \times \dot{V}_{CH_4}$) to CO_2 ratio at 450 °C.

achieved here is 0.13 sccm cm^{-2} without H_2 recycle and 0.25 sccm cm^{-2} with H_2 recycle, which translates to CH_4 production rates of 97 nmol s^{-1} cm^{-2} and 180 nmol s^{-1} cm^{-2}, respectively. In comparison, CH_4 production rates were reported to be ~ 0.05 nmol s^{-1} cm^{-2} using metal-nitrogen-doped carbon catalysts [40], 57 nmol s^{-1} cm^{-2} using a cobalt phthalocyanine and zinc–nitrogen–carbon tandem catalyst [41], and 3.9 nmol s^{-1} cm^{-2} with a polycrystalline Cu catalyst [42]. The higher CH_4 production rates provided by the PCEC directly improve system energy density to reduce capital costs, as can be seen in the techno-economic analysis presented later.

3.4. Comparison between electrochemical and thermochemical CH_4 production

The emergence of protons from the electrolyte into the CO_2-rich fuel electrode brings questions about the participation of activated H^+, in parallel with H_2, in the CO_2-to-CH_4 reaction pathway. To explore this further, we compared the co-conversion performance under electrochemically produced H_2 with that where the equivalent H_2 is co-fed with the CO_2 feedstock in the absence of an electrochemical driving current. The second approach treats the PCEC unit-cell stack as a fixed-bed reactor, where only thermochemically produced CH_4 is possible. The relative performances of the two CH_4-synthesis paths are plotted against $\dot{V}_{H_2,eq}$ and the results are shown in Fig. 8. It can be seen that the dependences of CO_2 conversion and CH_4 selectivity on the equivalent H_2 flow rate have altered. Perhaps most intriguingly, electrochemical synthesis results in higher overall CH_4 yields than chemical synthesis at operating temperatures ≥ 450 °C and low $\dot{V}_{H_2,eq}$ (for example, < 9 sccm at 450 °C) (Fig. 8c). The comparison was performed again using the cell with thicker electrolyte at 550 °C and a similar improvement during electrochemical synthesis can be observed (Fig. S9). This means that with the same materials set and morphology, the electrochemical formation of hydrogen increases methane yield, marking the existence of a possible EPOC effect in electrochemical CO_2 upgrade using PCEC.

In gaseous catalytic reactions, the EPOC effect is universally observed in both single-chamber and two-chamber (electrochemical cell) configurations for a variety of reactions [43]. With an oxygen-ion conductor support, the origin of EPOC in the oxidation process has

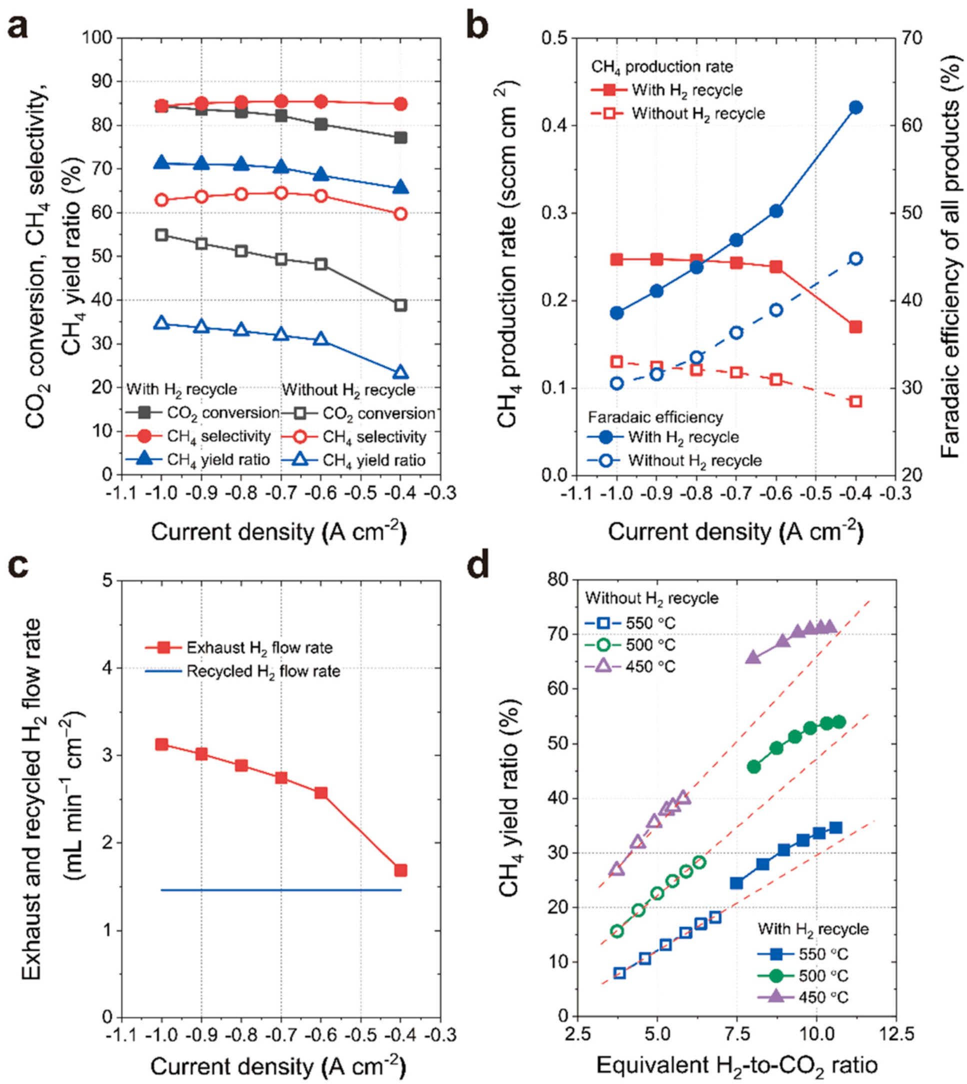

Fig. 7. In-situ CH_4 production during CO_2–H_2O co-conversion using the PCEC unit-cell stack with H_2 recycle simulated by feeding additional H_2 to the fuel electrode together with CO_2 at 450 °C. a, Change of CO_2 conversion, CH_4 selectivity and CH_4-yield ratio with current density; b, Change of CH_4 production rate and FE_{total} with current density. The FE_{total} is used instead of FE_{CH4}, as the formation of CH_4 contributed by the electrolyzed H_2 cannot be separated from the CH_4 production from recycled H_2; c, Comparison of flow rates of exhaust H_2 and recycled H_2, indicating that the additional H_2 feed can be fulfilled by exhaust H_2 recycle; d, Comparison of the CH_4-yield ratio between CO_2 upgrade with and without H_2 recycle against equivalent H_2 ($\dot{V}_{H_2,eq} = \dot{V}_{H_2} + \dot{V}_{CO} + 4 \times \dot{V}_{CH_4}$) to CO_2 ratio (Red dash lines are to guide the eyes only).

been found to stem from the migration of anionic $O^{\delta-}$ species from the support to the metal–gas interface, which alters the work function of the catalyst and serves as a sacrificial promoter to gas-phase O_2 reduction [44–47]. For the gaseous CO_2 hydrogenation process, catalysts supported with both oxygen-ion conducting electrolytes [26] and proton-conducting electrolytes [27,28] were demonstrated with electrochemically promoted catalytic performance. As in the thermochemical methanation of CO_2/CO, the rate-limiting process is generally ascribed to either the dissociation of the C–O bond or the hydrogenation of the intermediates [48,49]. In O-SOECs, through surface chemistry characterizations via *operando* photoelectron spectroscopy [50,51], the CO_2 electrolysis was suggested to go through a CO_3^{2-} intermediate. Upon anodic applied bias, the CO_3^{2-} intermediate accumulates, suggesting the promotion of the pre-coordination of CO_2 to the catalyst surface [50]. In PCECs, Shi, et al. [52] also observed the formation of CO_3^{2-} intermediates in the Ni-BZY fuel electrode, via in situ Raman and in situ diffuse reflectance infrared Fourier transform spectroscopy characterization. It was speculated that the continuously replenished protons play a critical role in the reduction of CO_2 in PCECs.

In this work, the CO_2 conversion was mainly promoted by the electrochemical route, while the CH_4 selectivity during electrochemical synthesis was equal to or lower than the thermochemical route, as revealed in Fig. 8a and b. Previously, Xie, et al. [23] also observed similar promotion on the CO_2 conversion with electrochemically produced H_2 using the protonic ceramic membrane as a hydrogen pump. The enhanced CO_2 conversion indicates a promoted formation of CO compared to conventional thermochemical processes involving molecular H_2. On the grounds of the above literature, two possible explanations can be raised. First, the applied bias and the protons may also facilitate the adsorption of CO_2 on the surface of Ni-BCZYYb fuel electrode as proposed by Yu, et a. [50] and subsequently drive the conversion from CO_3^{2-} to CO. From another perspective, the protons arriving at the fuel electrode might also work as a sacrificial promoter and directly participate in CO_2 reduction, schematically illustrated by the global hypothetical electrochemical CO_2 reduction (assuming a pure proton-conducting electrolyte):

$$CO_2 + 2H^+ + 2\,e^- = CO + H_2O\cdot \quad (5)$$

Additionally, the electric field present during electrochemical CO_2 reduction may increase the electrochemical potential of the combined H^+ and e^- and thus lower the transition state energy of the above reaction (Rx. 5). At lower temperatures and higher current densities, we hypothesize that H_2 evolution becomes increasingly favored and promotes the thermochemical route, while the EPOC effect brought by the applied bias and the protons is relatively less significant or even diminishing.

Admittedly, alternative possibilities such as contributions from partial oxygen-ion conductivity through the electrolyte or the different

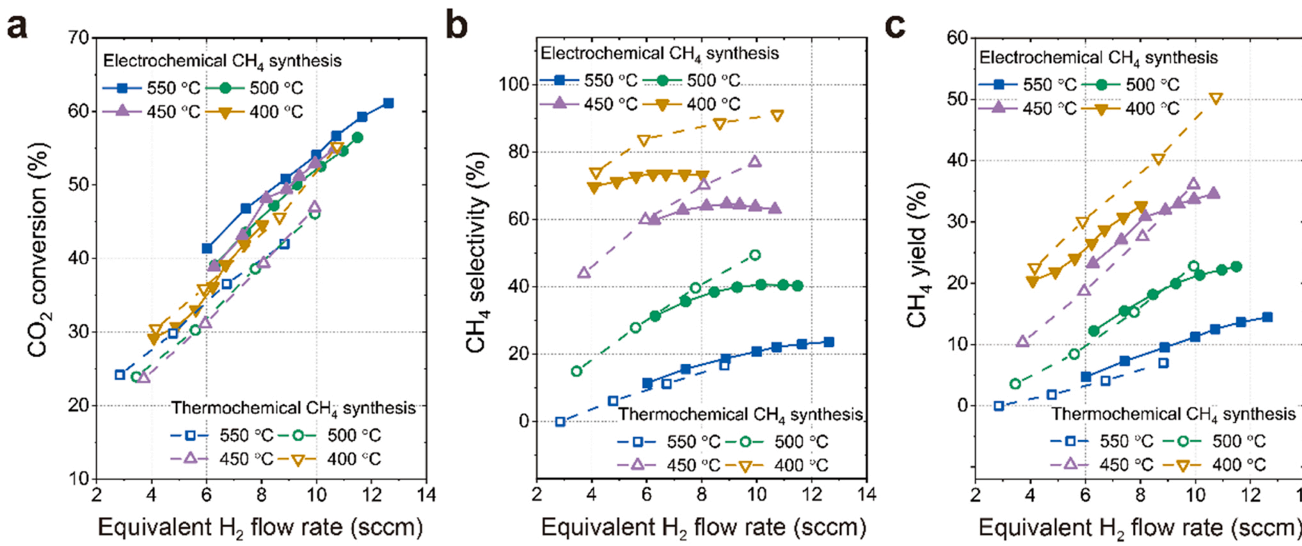

Fig. 8. Comparison between electrochemical CH_4 synthesis and thermochemical CH_4 synthesis. Thermochemical CH_4 synthesis was examined by co-feeding CO_2 and H_2 into the fuel-electrode chamber of the PCEC unit-cell stack in the absence of electrochemically produced H_2, using the stack as a fixed-bed reactor. All the panels are plotted as a function of the total equivalent H_2 flow rate($\dot{V}_{H_2,eq} = \dot{V}_{H_2} + \dot{V}_{CO} + 4 \times \dot{V}_{CH_4}$), in the exhaust gas. a–c, CO_2 conversion, CH_4 selectivity and CH_4 yield as a function of $\dot{V}_{H_2,eq}$. Generally, electrochemical CH_4 synthesis outperforms thermochemical CH_4 synthesis at high temperatures ($\geq$ 450 °C) and low $\dot{V}_{H_2,eq}$ (for example, < 9 sccm at 450 °C).

location of the H_2 source cannot be ruled out. Nonetheless, if an EPOC effect in PCECs can be validated, it would reinforce the potential benefits of integrating CH_4 synthesis and electrochemical CO_2–H_2O co-conversion in a single step. This would also suggest that similar proton-mediated electrochemical processes could potentially be harnessed to promote the activity of other hydrogenation reactions, such as the Haber–Bosch process for ammonia synthesis [53,54].

3.5. Techno-economic of CO_2 upgrading to CH_4-based product gas with PCECs

We have pursued the techno-economic analysis of electrochemically upgrading CO_2 into CH_4-based product gas to determine system-scale operating conditions and guide technological development. Levelized cost of fuel production (LCOFP) quantifies the required price-point of the product gas to enable "break-even" plant costs at the end of plant life (Eq. S4), presenting an insightful method for comparing the economics of various technologies. A PCEC-based plant model for CO_2 upgrade is shown in Fig. S10. LCOFP was compared across four operational state points detailed in Table S4. Detailed modeling process information can be found in the Supplemental Experimental Procedures. Economic assumptions can be found in Table S5.

LCOFPs for the four cases are compared in Fig. 9. Electricity cost is clearly the major contributor to total LCOFP, reflective of the energy required to co-convert the CO_2 and H_2O into fuels. For the baseline case (Case 1, related to Fig. 4), all hydrogen is produced through H_2O electrolysis; no H_2 recycle is used. The LCOFP is 588 $\$_{2020}$ MWh^{-1}. The mildly oxidizing gas compositions bring low FE_{total} (~ 30%), increasing both capital and operational costs.

Case 2 explores the impact of electrolyte thickness on LCOFP; the increased thickness boosts FE_{total} from 30% to 40%, but necessitates a higher driving voltage to achieve the –1 A cm^{-2} current density. Overall, increasing the electrolyte thickness only mildly reduces the LCOFP from 588 $\$_{2020}$ MWh^{-1} to 579 $\$_{2020}$ MWh^{-1}. The gains in the increasing CH_4-yield ratio are partially offset by the higher power required.

The value proposition of H_2 recycle is captured in Case 3. LCOFP decreases substantially under H_2 recycle (Case 3), dropping to 223 $\$_{2020}$ MWh^{-1}, less than half the baseline case. Recycling unconsumed H_2 could substantially improve the CH_4 production rate per unit area of the PCEC stack (Fig. 7b). In addition, the more-reducing gas conditions brought by H_2 recycle greatly lower hole conduction, increasing the FE_{total}. The higher FE_{total} and increased areal CH_4 production rate enabled by H_2 recycle more than halves the electricity costs, and also reduces capital cost. Mass and energy balances for Case 3 can be found in Table S6. Cost contributions for Case 3 excluding charging cost are shown in Fig. S11.

The economics of fuel production rely heavily on economic factors,

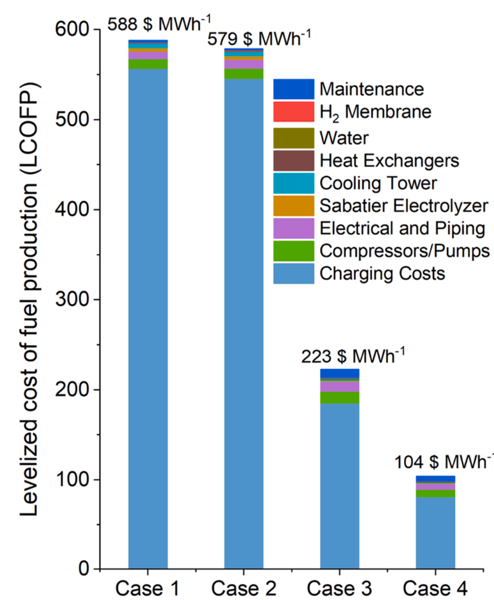

Fig. 9. Levelized cost of fuel production (LCOFP) analysis of the proposed CO_2 upgrading plant based on PCEC technology. Detailed modeling process can be found in the Supplemental Experimental Procedures. Case 1 (Related to Fig. 4) and Case 2 (Related to Fig. S7, with thicker electrolyte) are without exhaust H_2 recycle, while Case 3 (Related to Fig. 7) is with exhaust H_2 recycle. The PCEC plant presents LCOFPs of 579 $\$_{2020}$ MWh^{-1} without H_2 recycle (Case 2) and 223 $\$_{2020}$ MWh^{-1} with H_2 recycle (Case 3). Further increasing the Faradaic efficiency to 90% and lowering the electricity cost to 0.02 \$ kWh^{-1} (Case 4) lead to an LCOFP of 104 $\$_{2020}$ MWh^{-1}.

such as electricity cost, and on technical indicators, such as the FE_{total}. Fig. S12a shows the cost breakdowns and the impact of FE_{total} on the LCOFP at a fixed electricity cost of 0.05 \$ kWh^{-1}. PCEC performance with increasing FE_{total} was projected by holding the H_2-to-CO_2 ratio, as well as other salient performance metrics – CO_2 conversion and CH_4 selectivity – constant. By increasing the FE_{total} from 62.1% to 100%, the LCOFP is reduced by 28% to 161 $\$_{2020}$ MWh^{-1}. The impact of electricity cost on LCOFP is captured in Fig. S12b at a fixed FE_{total} of 62.1%. By decreasing the electricity cost from 0.05 \$ kWh^{-1} to 0.01 \$ kWh^{-1}, the LCOFP is further reduced by 58% to 93 $\$_{2020}$ MWh^{-1}.

The synergistic effect of the electricity cost and the FE_{total} on LCOFP is shown in Fig. S13. When matching a low electricity cost of 0.02 \$ kWh^{-1} with high FE_{total} of 90%, the LCOFP drops to 104 $\$_{2020}$ MWh^{-1} (Fig. 9, Case 4). Such operating conditions are reasonable; in a previous report, Duan, et al. [14] demonstrated FE of over 90% during water electrolysis using a similar PCEC materials set. Further, the U.S. Department of Energy (DoE) has set a new goal of driving down the current cost of solar electricity to 0.02 \$ kWh^{-1} by 2030 [55]. Thus, cost-effective CO_2 conversion to CH_4 is possible through a combination of advancements in renewables technologies and PCEC materials. Further materials advancements to reduce electronic conductivity in protonic ceramics and improve catalytic activity would clearly be of value.

4. Conclusions

In this work, we have experimentally demonstrated a promising protonic-ceramic electrolysis cell for direct electrochemical co-conversion of CO_2–H_2O to methane. The important tradeoffs between operating conditions and performance metrics were explored from a broader viewpoint of system-level practicability using a PCEC unit-cell stack. Paths to significantly improve the CH_4-yield ratio were demonstrated and the highest CH_4-yield ratio of 34.6% by direct electrolytic co-conversion of CO_2–H_2O feedstocks was achieved at 450 °C. Co-feeding H_2 with CO_2 boosts the CH_4-yield ratio to 71.2%. This supplemental hydrogen can be recycled from the reactor exhaust stream, where unused electrochemically produced H_2 can be harvested, eliminating a need for any external H_2 supply. In addition, we find that electrochemical CH_4 synthesis presents a possible EPOC phenomenon that results in a higher CH_4-yield ratio than thermochemical CH_4 synthesis at high temperatures and low equivalent hydrogen flow rates. This could be ascribed to either faster CO_2 adsorption or work function alteration of the electrode by the protons acting as a sacrificial promoter under applied bias. The performance of the protonic ceramic cell was also evaluated under fuel-cell mode. With diluted CH_4 as the fuel, a peak power density of 0.22 W cm^{-2} was achieved at 550 °C. The techno-economic analysis projects the LCOFP by electrochemical CO_2 upgrading with PCECs of 104 $\$_{2020}$ MWh^{-1} at a favorable condition with a target Faradaic efficiency of 90% and an electricity cost of 0.02 \$ kWh^{-1}. This study demonstrates a promising result for future scale-up and practical application of PCECs in electrochemical CO_2 upgrading as a potential grid-balancing solution.

CRediT authorship contribution statement

Zehua Pan: Conceptualization, Data curation, Formal analysis, Investigation, Methodology, Writing – original draft, Writing – review & editing, Visualization. **Chuancheng Duan:** Conceptualization, Methodology, Writing – original draft, Writing – review & editing. **Tyler Pritchard:** Methodology, Formal analysis, Investigation. **Amogh Thatte:** Methodology. **Erick White:** Funding acquisition, Writing – review & editing. **Robert Braun:** Methodology, Funding acquisition, Writing – review & editing. **Ryan O'Hayre:** Conceptualization, Supervision, Funding acquisition, Writing – review & editing. **Neal P. Sullivan:** Conceptualization, Supervision, Funding acquisition, Writing – review & editing.

Declaration of Competing Interest

The authors declare that they have no known competing financial interests or personal relationships that could have appeared to influence the work reported in this paper.

Acknowledgement

This material is based upon work supported by the Department of Energy, USA, under Award Number DE-FE0031716. The authors gratefully appreciate Sami El Hageali and Long Le for the discussions in cell fabrication and test stand set-up. This report was prepared as an account of work sponsored by an agency of the United States Government. Neither the United States Government nor any agency thereof, nor any of their employees, makes any warranty, express or implied, or assumes any legal liability or responsibility for the accuracy, completeness, or usefulness of any information, apparatus, product, or process disclosed, or represents that its use would not infringe privately owned rights. Reference herein to any specific commercial product, process, or service by trade name, trademark, manufacturer, or otherwise does not necessarily constitute or imply its endorsement, recommendation, or favoring by the United States Government or any agency thereof. The views and opinions of authors expressed herein do not necessarily state or reflect those of the United States Government or any agency thereof.

Appendix A. Supporting information

Supplementary data associated with this article can be found in the online version at doi:10.1016/j.apcatb.2022.121196.

References

[1] Y. Zheng, et al., A review of high temperature co-electrolysis of H_2O and CO_2 to produce sustainable fuels using solid oxide electrolysis cells (SOECs): advanced materials and technology, Chem. Soc. Rev. 46 (5) (2017) 1427–1463.
[2] S. Park, et al., In situ exsolved Co nanoparticles on Ruddlesden-Popper material as highly active catalyst for CO_2 electrolysis to CO, Appl. Catal. B: Environ. 248 (2019) 147–156.
[3] D.M. Bierschenk, J.R. Wilson, S.A. Barnett, High efficiency electrical energy storage using a methane–oxygen solid oxide cell, Energy Environ. Sci. 4 (3) (2011) 944–951.
[4] E.P. Reznicek, R.J. Braun, Reversible solid oxide cell systems for integration with natural gas pipeline and carbon capture infrastructure for grid energy management, Appl. Energy 259 (2020), 114118.
[5] C.H. Wendel, P. Kazempoor, R.J. Braun, A thermodynamic approach for selecting operating conditions in the design of reversible solid oxide cell energy systems, J. Power Sources 301 (2016) 93–104.
[6] W.L. Becker, M. Penev, R.J. Braun, Production of synthetic natural gas from carbon dioxide and renewably generated hydrogen: a techno-economic analysis of a power-to-gas strategy, J. Energy Resour. Technol. 141 (2) (2019).
[7] C. Duan, et al., Proton-conducting oxides for energy conversion and storage, Appl. Phys. Rev. 7 (1) (2020), 011314.
[8] C.H. Wendel, R.J. Braun, Design and techno-economic analysis of high efficiency reversible solid oxide cell systems for distributed energy storage, Appl. Energy 172 (2016) 118–131.
[9] W. Li, et al., Performance and methane production characteristics of H_2O–CO_2 co-electrolysis in solid oxide electrolysis cells, Int. J. Hydrog. Energy 38 (25) (2013) 11104–11109.
[10] K. Xie, et al., Direct synthesis of methane from CO_2/H_2O in an oxygen-ion conducting solid oxide electrolyser, Energy Environ. Sci. 4 (6) (2011) 2218.
[11] Y. Luo, et al., Experimental characterization and theoretical modeling of methane production by H_2O/CO_2 co-electrolysis in a tubular solid oxide electrolysis cell, J. Electrochem. Soc. 162 (10) (2015) F1129–F1134.
[12] L. Chen, F. Chen, C. Xia, Direct synthesis of methane from CO_2–H_2O co-electrolysis in tubular solid oxide electrolysis cells, Energy Environ. Sci. 7 (12) (2014) 4018–4022.
[13] L. Lei, et al., The co-electrolysis of CO_2–H_2O to methane via a novel micro-tubular electrochemical reactor, J. Mater. Chem. A 5 (6) (2017) 2904–2910.
[14] C. Duan, et al., Highly efficient reversible protonic ceramic electrochemical cells for power generation and fuel production, Nat. Energy 4 (3) (2019) 230–240.
[15] S. Choi, T.C. Davenport, S.M. Haile, Protonic ceramic electrochemical cells for hydrogen production and electricity generation: exceptional reversibility, stability, and demonstrated faradaic efficiency, Energy Environ. Sci. 12 (1) (2019) 206–215.
[16] E. Vollestad, et al., Mixed proton and electron conducting double perovskite anodes for stable and efficient tubular proton ceramic electrolysers, Nat. Mater. 18 (7) (2019) 752–759.

[17] L.Q. Le, et al., Proton-conducting ceramic fuel cells: scale up and stack integration, J. Power Sources 482 (2021), 228868.
[18] N. Shi, et al., Co-generation of electricity and olefin via proton conducting fuel cells using $(Pr_{0.3}Sr_{0.7})_{0.9}Ni_{0.1}Ti_{0.9}O_3$ catalyst layers, Appl. Catal. B: Environ. 272 (2020), 118973.
[19] S.H. Morejudo, et al., Direct conversion of methane to aromatics in a catalytic co-ionic membrane reactor, Science 353 (6299) (2016) 563–566.
[20] C. Vogt, et al., The renaissance of the sabatier reaction and its applications on Earth and in space, Nat. Catal. 2 (3) (2019) 188–197.
[21] S. Walspurger, et al., Sorption enhanced methanation for substitute natural gas production: Experimental results and thermodynamic considerations, Chem. Eng. J. 242 (2014) 379–386.
[22] H. Ohya, et al., Methanation of carbon dioxide by using membrane reactor integrated with water vapor permselective membrane and its analysis, J. Membr. Sci. 131 (1–2) (1997) 237–247.
[23] K. Xie, et al., Electrochemical reduction of CO_2 in a proton conducting solid oxide electrolyser, J. Mater. Chem. 21 (1) (2011) 195–198.
[24] M. Li, et al., Switching of metal–oxygen hybridization for selective CO_2 electrohydrogenation under mild temperature and pressure, Nat. Catal. 4 (4) (2021) 274–283.
[25] A. Katsaounis, Recent developments and trends in the electrochemical promotion of catalysis (EPOC), J. Appl. Electrochem. 40 (5) (2010) 885–902.
[26] V. Jiménez, et al., Electrochemical promotion of the CO_2 hydrogenation reaction on composite Ni or Ru impregnated carbon nanofiber catalyst-electrodes deposited on YSZ, Appl. Catal. B: Environ. 107 (1–2) (2011) 210–220.
[27] D. Zagoraios, et al., Electrochemical promotion of Ru nanoparticles deposited on a proton conductor electrolyte during CO_2 hydrogenation, Appl. Catal. B: Environ. 276 (2020), 119148.
[28] I. Kalaitzidou, et al., Electrochemical promotion of the hydrogenation of CO_2 on Ru deposited on a BZY proton conductor, J. Catal. 331 (2015) 98–109.
[29] C. Duan, et al., Readily processed protonic ceramic fuel cells with high performance at low temperatures, Science 349 (6254) (2015) 1321–1326.
[30] D. Konwar, H.H. Yoon, A methane-fueled SOFC based on a thin $BaZr_{0.1}Ce_{0.7}Y_{0.1}Yb_{0.1}O_{3-\delta}$ electrolyte film and a $LaNi_{0.6}Co_{0.4}O_3$ anode functional layer, J. Mater. Chem. A 4 (14) (2016) 5102–5106.
[31] C. Duan, et al., Highly durable, coking and sulfur tolerant, fuel-flexible protonic ceramic fuel cells, Nature 557 (7704) (2018) 217–222.
[32] K.D. Kreuer, On the development of proton conducting materials for technological applications, Solid State Ion. 97 (1) (1997) 1–15.
[33] H. Zhu, et al., Defect chemistry and transport within dense $BaCe_{0.7}Zr_{0.1}Y_{0.1}Yb_{0.1}O_{3-\delta}$ (BCZYYb) proton-conducting membranes, J. Electrochem. Soc. 165 (10) (2018) F845–F853.
[34] H. Zhu, et al., Defect incorporation and transport within dense $BaZr_{0.8}Y_{0.2}O_{3-\delta}$ (BZY20) proton-conducting membranes. J. Electrochem. Soc. 165 (9) (2018) F581–F588.
[35] T. Somekawa, et al., Physicochemical properties of proton-conductive Ba $(Zr_{0.1}Ce_{0.7}Y_{0.1}Yb_{0.1})O_{3-\delta}$ solid electrolyte in terms of electrochemical performance of solid oxide fuel cells, Int. J. Hydrog. Energy 41 (39) (2016) 17539–17547.
[36] H. Zhu, R.J. Kee, Membrane polarization in mixed-conducting ceramic fuel cells and electrolyzers, Int. J. Hydrog. Energy 41 (4) (2016) 2931–2943.
[37] T. Nakamura, et al., Energy efficiency of ionic transport through proton conducting ceramic electrolytes for energy conversion applications, J. Mater. Chem. A 6 (32) (2018) 15771–15780.
[38] R. Qiu, et al., Multifactor theoretical analysis of current leakage in proton-conducting solid oxide fuel cells, J. Power Sources 505 (2021), 230038.
[39] Q. Zhang, Y. Guo, J. Ding, Characterization of the conductivity distribution and leakage current in proton-conducting ceramic electrolyte through modeling and sensitivity analysis, Int. J. Hydrog. Energy 46 (61) (2021) 31370–31381.
[40] A.S. Varela, et al., Electrochemical reduction of CO_2 on metal-nitrogen-doped carbon catalysts, ACS Catal. 9 (8) (2019) 7270–7284.
[41] L. Lin, et al., Enhancing CO_2 electroreduction to methane with a cobalt phthalocyanine and zinc-nitrogen-carbon tandem catalyst, Angew. Chem. Int. Ed. Engl. (2020).
[42] M.T. Tang, et al., From electricity to fuels: descriptors for C1 selectivity in electrochemical CO_2 reduction, Appl. Catal. B: Environ. 279 (2020), 119384.
[43] C.G. Vayenas, et al., Electrochemical Activation of Catalysis: Promotion, Electrochemical Promotion, and Metal-support Interactions, Springer, 2001.
[44] A. Katsaounis, et al., Comparative isotope-aided investigation of electrochemical promotion and metal–support interactions: 2. CO oxidation by $18O_2$ on electropromoted Pt films deposited on YSZ and on nanodispersed Pt/YSZ catalysts, J. Catal. 226 (1) (2004) 197–209.
[45] X. Li, F. Gaillard, P. Vernoux, Investigations under real operating conditions of the electrochemical promotion by O_2 temperature programmed desorption measurements, Top. Catal. 44 (3) (2007) 391–398.
[46] A. Nakos, S. Souentie, A. Katsaounis, Electrochemical promotion of methane oxidation on Rh/YSZ, Appl. Catal. B: Environ. 101 (1) (2010) 31–37.
[47] M.N. Tsampas, et al., Isotopical labeling mechanistic studies of electrochemical promotion of propane combustion on Pt/YSZ, Electrochem. Commun. 26 (2013) 13–16.
[48] W. Wang, et al., Recent advances in catalytic hydrogenation of carbon dioxide, Chem. Soc. Rev. 40 (7) (2011) 3703–3727.
[49] B. Miao, et al., Catalysis mechanisms of CO_2 and CO methanation, Catal. Sci. Technol. 6 (12) (2016) 4048–4058.
[50] Y. Yu, et al., CO_2 activation and carbonate intermediates: an operando AP-XPS study of CO_2 electrolysis reactions on solid oxide electrochemical cells, Phys. Chem. Chem. Phys. 16 (23) (2014) 11633–11639.
[51] A.K. Opitz, et al., Surface Chemistry of Perovskite-Type Electrodes During High Temperature CO_2 Electrolysis Investigated by Operando Photoelectron Spectroscopy, ACS Appl. Mater. Interfaces 9 (41) (2017) 35847–35860.
[52] N. Shi, et al., Controllable CO_2 conversion in high performance proton conducting solid oxide electrolysis cells and the possible mechanisms, J. Mater. Chem. A 7 (9) (2019) 4855–4864.
[53] V. Kyriakou, et al., An electrochemical haber-bosch process, Joule 4 (1) (2020) 142–158.
[54] W. Guo, et al., Electrochemical nitrogen fixation and utilization: theories, advanced catalyst materials and system design, Chem. Soc. Rev. 48 (24) (2019) 5658–5716.
[55] DOE Announces Goal to Cut Solar Costs by More than Half by 2030. 2021; Available from: ⟨https://www.energy.gov/articles/doe-announces-goal-cut-solar-costs-more-half-2030⟩.